European Journal of Pharmaceutics and Biopharmaceutics 75 (2010) 341–353

Contents lists available at ScienceDirect

European Journal of Pharmaceutics and Biopharmaceutics

journal homepage: www.elsevier.com/locate/ejpb

Research paper

Enhanced antitumor efficacy by Paclitaxel-loaded Pluronic P123/F127 mixed micelles against non-small cell lung cancer based on passive tumor targeting and modulation of drug resistance

Zhang Wei [a], Shi Yuan [b], Yanzuo Chen [a], Shuangyin Yu [a], Junguo Hao [a], Jieqi Luo [a], Xianyi Sha [a], Xiaoling Fang [a,*]

[a] School of Pharmacy, Fudan University, Shanghai, China
[b] Shanghai Hengrui Pharmaceuticals Co., Ltd., Shanghai, China

ARTICLE INFO

Article history:
Received 19 January 2010
Accepted in revised form 29 April 2010
Available online 6 May 2010

Keywords:
Polymeric micelles
Paclitaxel
Pluronic
A-549
Multidrug resistance

ABSTRACT

The aim of this work was to demonstrate the advantage of using paclitaxel (PTX)-loaded Pluronic P123/F127 mixed micelles (PF-PTX) against non-small cell lung cancer (NSCLC) compared to Taxol. Modulation of multidrug resistance (MDR) by Pluronic mixed micelles was evaluated in lung resistance protein (LRP)-overexpressing human lung adenocarcinoma A-549 cell line. Influence of PF-PTX on in vitro cytotoxicity was determined by MTT assay, while cellular apoptosis was detected by cell nuclei staining and Annexin V-FITC apoptosis detection kit. Cell cycle arrest was also confirmed by flow cytometry. Additionally, in vivo fate and antitumor efficacy of PF-PTX were extensively evaluated in comparison with Taxol. It was demonstrated that PF-PTX had superior anti-proliferation activity against A-549 cells compared with Taxol as measured by IC_{50}. The enhanced anti-cancer efficacy of PF-PTX was associated with PTX-induced apoptosis and cell arrest in the G_2/M phase. Intracellular ATP depletion and decreased mitochondrial potential caused by Pluronic copolymers were found to be related to modulation of MDR. PF-PTX also exhibited significant advantages in pharmacokinetics and A-549 xenograft tumor model *versus* Taxol. The PF-PTX formulation achieved 3.0-fold longer mean residence time in circulation, 2.2-fold larger area under the plasma concentration–time curve than Taxol. At 28 days, tumor volume in PF-PTX group was only 31.8% that of the Taxol. Therefore, PF-PTX significantly enhanced the anti-cancer activity of PTX and might be considered a promising drug delivery system to overcome MDR in lung cancer.

1. Introduction

Lung cancer is the leading cause of cancer-related deaths throughout the world, with a higher annual death rate than prostate, colon and breast cancers combined and a dismal 5-year survival rate of 15% [1]. Non-small cell lung cancer (NSCLC) comprises approximately 75–80% of all lung cancers. It is well known that multidrug resistance (MDR) is a major obstacle in the chemotherapy of NSCLC. Clinically, several resistance proteins, including P-glycoprotein (P-gp), lung resistance protein (LRP) and multidrug resistance-associated protein (MRP), are proved to be simultaneously involved in MDR of NSCLC [2,3]. Take human lung adenocarcinoma A-549 cell line for example, a high expression level of LRP was detected at the nuclear envelope and cytoplasm in A-549 cells [4], and it was investigated that LRP was involved in resistance to doxorubicin, paclitaxel, vincristine and etoposide [5]. Additionally, a number of ATP-binding cassette (ABC) efflux pumps such as P-gp, MRP and breast cancer resistance protein (BCRP) were also reported in A-549 cells [6–9]. Taken together, we use A-549 cell line as a lung MDR tumor cell model in the study for further in vitro and in vivo investigation [10].

Paclitaxel (PTX) that works by interfering with normal microtubule breakdown during cell division has been one of the most successful anti-cancer drugs and has shown its potency against a broad spectrum of cancers, especially against NSCLC, metastatic breast cancer and refractory ovarian cancer [11,12]. However, because of the poor aqueous solubility and low therapeutic index of PTX, its clinical application is extremely limited. One commercial preparation of PTX is Taxol, a concentrated solution composed of a 50:50 (v/v) mixture of Cremophor EL (polyoxyl 35 castor oil) and dehydrated alcohol, which is diluted 5–20-fold in normal saline or dextrose solution before administration. Unfortunately, serious side effects attributable to Cremophor EL, such as hypersensitivity, nephrotoxicity and neurotoxicity have been reported [13]. To overcome the problems caused by Cremophor EL and to improve the drug efficacy, some research work has been focused

* Corresponding author. School of Pharmacy, Fudan University, Lane 826, Zhangheng Road, Shanghai 201203, China. Tel.: +86 21 51980071; fax: +86 21 51980072.
E-mail address: xlfang@shmu.edu.cn (X. Fang).

0939-6411/$ - see front matter Crown Copyright © 2010 Published by Elsevier B.V. All rights reserved.
doi:10.1016/j.ejpb.2010.04.017

on developing new drug delivery systems. Several new formulations of PTX are in clinical trials or also marketed. Abraxane, an injectable suspension of albumin-bound PTX nanoparticles, is approved for use in patients with metastatic breast cancer or relapse within 6 months of adjuvant chemotherapy [14]; One novel formulation of PTX is Genexol-PM (Samyang Co., Seoul, Korea), a form of PTX formulated with sterile, lyophilized polymeric micelles that allow intravenous delivery of PTX without Cremophor EL. Additionally, Genexol-PM has already reached Phase II stage and appears a promising new PTX in view of significant efficacies [15]. However, PTX resistance is found in more than 70% of patients at the time of initial diagnosis and almost in all patients upon relapse [16].

It has been reported that the common causes for MDR include overexpression of membrane spanning ATP-dependent drug efflux pumps from the ABC transporter family (most notably P-glycoprotein, P-gp), modifications in drug metabolism through glutathione-S-transferase or cytochrome P450 activity, alterations in DNA repair mechanisms and modifications in apoptotic signaling [17,18]. For this purpose, formulation strategies, including colloidal delivery systems such as liposomes, nanocapsules and nanoparticles [19–23], polymer–drug conjugates [24,25] and polymeric micelles [26,27], have been developed to potentially overcome MDR tumors. These multi-functional nanocarriers are developed to enhance drug delivery and overcome MDR by either simultaneous or sequential delivery of resistance modulators (P-gp substrates), agents that regulate intracellular pH, agents that lower the apoptotic threshold (ceramide and curcumin) or in combination with energy delivery (sound, heat and light) to enhance the effectiveness of anti-cancer agents in refractory tumors [28]. One promising nanomedicine-based technology is polymeric micelles, which have been evaluated in several clinical trials as carriers for anti-cancer drugs [29–32]. In particular, doxorubicin-loaded mixed micelles composed of Pluronic L61 and F127 (SP1049C) have already reached Phase III stage [33].

Moreover, recent developments indicate that selecting proper polymer nanomaterials can implement more than one inert carrier function by being biological response modifiers [34]. One representative of such materials is Pluronic block copolymers that are amphiphilic synthetic polymers containing hydrophilic poly(ethylene oxide) (PEO) blocks and hydrophobic poly(propylene oxide) (PPO) blocks arranged in triblock structure: PEO–PPO–PEO. It has been reported to inhibit the P-gp efflux system by ATP depletion in MDR cancer cells, as well as to reduce the glutathione/glutathione-S-transferase detoxification system and to alter apoptotic signal transduction. However, very little research has investigated the use of Pluronic polymeric micelles as both drug nanocarrier and MDR modulator. Therefore, to combine the MDR tumor-sensitizing properties of Pluronic copolymers with the long circulation effect of Pluronic polymeric micelles, we previously developed PTX-loaded Pluronic P123/F127 mixed polymeric micelles (PF-PTX) [35]. In this study, we attempted to perform a systematic evaluation of the antitumor efficacy of PF-PTX by performing intracellular accumulation, subcellular distribution, in vitro cytotoxicity, cellular apoptosis and cell cycle assay in A-549 cells and an in vivo study in xenograft nude mice model.

2. Materials and methods

2.1. Materials and animals

Paclitaxel was purchased from Xi'an Sanjiang Bio-Engineering Co., Ltd. (Xi'an, China). Samples of Pluronic P123, F127 and Cremophor EL were kindly supplied by BASF Ltd. (Shanghai, China). Taxol injection (prepared according to the commercial formulation of Taxol). 3-(4,5-dimethyl-thiazol-2-yl)-2,5-diphenyl-tetrazolium bromide (MTT) and trinitrobenzenesulfonic acid (TNBS) were purchased from Sigma (St. Louis, MO, USA). Penicillin–streptomycin, RPMI 1640, fetal bovine serum (FBS) and 0.25% (w/v) trypsin–0.03% (w/v) EDTA solution were purchased from Gibco BRL (Gaithersberg, MD, USA). RNase A, propidium iodide (PI), rhodamine B isothiocyanate (RITC) and Hoechst 33342 were purchased from Sigma (St. Louis, MO, USA). Micro BCA Protein assay kit, Annexin V-FITC Apoptosis Detection kit, ATP assay kit, Mitochondrial membrane potential assay kit with JC-1, MitoTracker Green and TritonX-100 were purchased from Beyotime® Biotechnology Co., Ltd. (Nantong, China). Purified deionized water was prepared by the Milli-Q plus system (Millipore Co., Billerica, MA, USA). All other reagents and chemicals were of analytical grade and were used without further purification.

The lung resistance protein (LRP)-overexpressing human lung tumor cell line A-549 was obtained from the Institute of Biochemistry and Cell Biology, Shanghai Institutes for Biological Sciences, Chinese Academy of Sciences (Shanghai, China). The cells were cultured in RPMI 1640 medium, supplemented with 10% FBS, 100 IU/ml penicillin and 100 μg/ml streptomycin sulfate. All the cells were cultured in incubators maintained at 37 °C with 5% CO_2 under fully humidified conditions. All experiments were performed on cells in the logarithmic phase of growth.

Male Sprague–Dawley (SD) rats (220 ± 20 g), Kunming strain mice (20 ± 2 g), and male BALB/c nude mice (22 ± 2 g), supplied by Department of Experimental Animals, Fudan University (Shanghai, China), were acclimated at 25 °C and 55% of humidity under natural light/dark conditions for 1 week before dosing. All animal experiments were carried out in accordance with guidelines evaluated and approved by the ethics committee of Fudan University (Shanghai, China).

2.2. Synthesis of RITC-Pluronic P123

2.2.1. Synthesis of amino-terminated Pluronic P123

Amino-terminated P123 (P123-NH_2) was synthesized by a modified procedure as described earlier [36]. Briefly, Pluronic P123 was purified by dissolving in acetone and precipitating into an excess amount of cooled hexane and dried under vacuum. The purified Pluronic P123 (5.75 g, 1 mmol) was dissolved in dry acetonitrile (15 ml) and added dropwise to an excess amount of *N,N′*-carbonyldiimidazole (CDI) (1.62 g, 10 mmol) in dry acetonitrile (15 ml) at room temperature during a 2-h period under nitrogen atmosphere. After the addition, the mixture was kept stirring for an additional 2 h. After reaction, the mixture was treated with 0.2 mL of water for 20 min to neutralize the nonreacted CDI and then added dropwise to 10 ml of 1,2-ethylenediamine at room temperature in 2 h. The mixture was allowed to react overnight. The unreacted 1,2-ethylenediamine was removed by evaporation, and the resulting viscous oil was dialyzed for 5 days against water. Finally, the dialyzed solution was freeze-dried to yield P123-NH_2 (4.86 g, 84.5%). As shown in Fig. 1A, 1H NMR spectrum (400 MHz, $CDCl_3$, ppm) of P123-NH_2 showed the peaks at δ (ppm) = 1.02 (d, 3H × 69, $-CH_3$ of PPO), 3.40–3.50 (m, 3H × 69, 4H × 40, $-CH_2CHO$ of PPO and $-CH_2CH_2O-$ of PEO), 2.75 (t, 2H × 2, $-CH_2N$), 3.20 (q, 2H × 2, $CNCH_2-$). FT-IR spectrum of P123-NH_2 confirmed the presence of carbonyl groups in the polymer chain (1765 cm^{-1}, data not shown). Furthermore, trinitrobenzenesulfonic acid (TNBS) assay for amino groups also confirmed that 94.02% of P123 terminals were conjugated with amino groups.

2.2.2. Synthesis of RITC-Pluronic P123

The lyophilized P123-NH_2 (0.25 g, 42 μmol) was added to 67.5 mg (126 μmol) of RITC in 10 ml DMF and stirred in a nitrogen atmosphere at room temperature in the dark overnight. Then, the

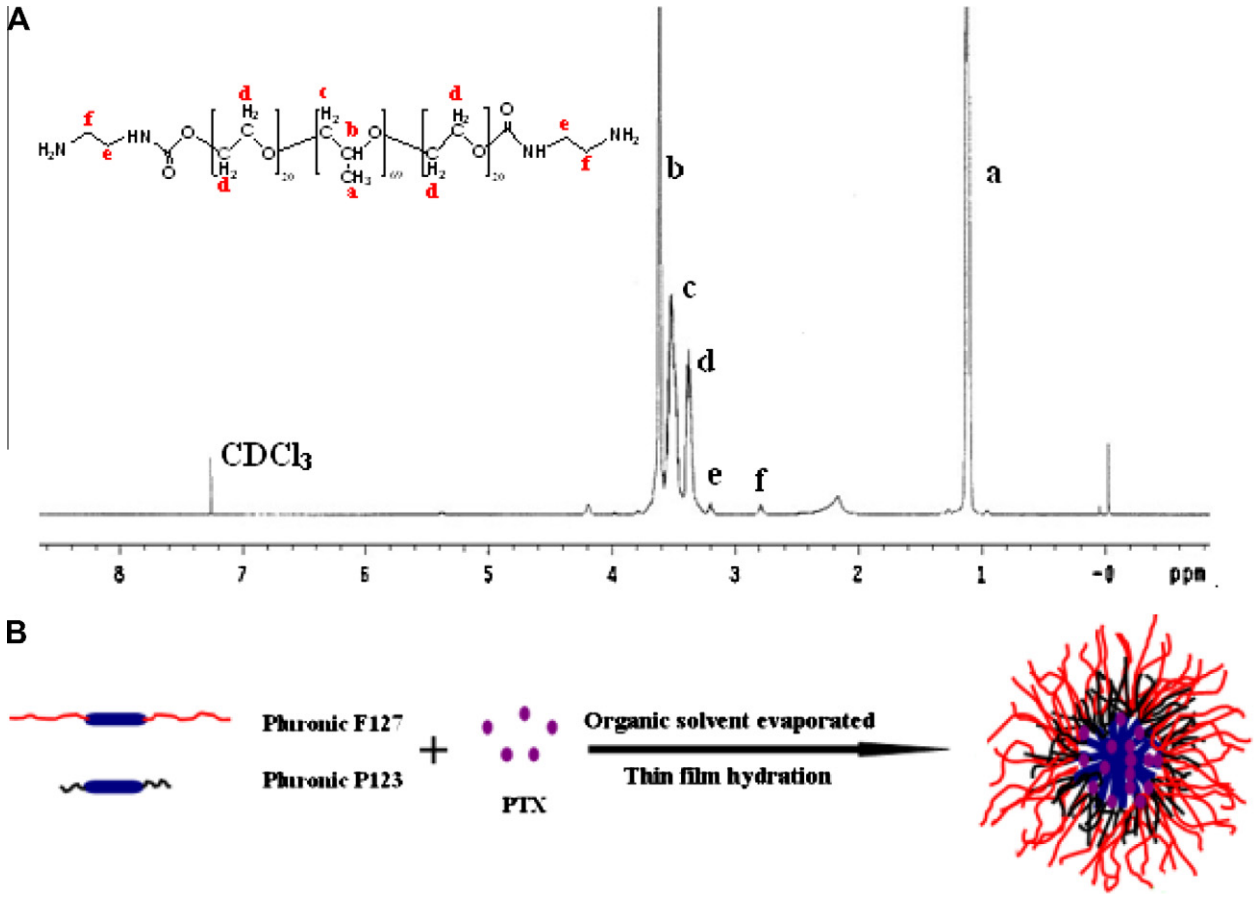

Fig. 1. (A) The ^{1}H NMR spectrum of P123-NH_2. (B) Representation of the strategy of developing Pluronic P123/F127 mixed polymeric micelles. (For interpretation of the references to colour in this figure legend, the reader is referred to the web version of this article.)

mixture was subsequently dialyzed (MWCO 3500) for a week against weakly alkaline aqueous solution (pH 8.0). RITC-labeled Pluronic P123 was obtained by freeze-drying. The conjugation percentage was calculated by determining the amount of RITC conjugated in RITC-P123. A known amount of lyophilized RITC-P123 was dissolved in ethanol, and a UV absorbance value at 550 nm was measured to determine the concentration of conjugated RITC. Serially diluted concentrations of RITC in ethanol were used to construct a calibration curve. The conjugation percentage of RITC to Pluronic P123 was 82.37% on a molar ratio basis.

2.3. Preparation and characterization of PF-PTX polymeric micelles

PF-PTX polymeric mixed micelles were prepared by thin-film hydration method as described earlier [35] (Fig. 1B). Briefly, 4 mg of PTX and 270 mg of Pluronic mixture composed of P123 and F127 (2:1, w/w) were dissolved in 10-ml acetonitrile in a round-bottom flask. The solvent was evaporated by rotary evaporation at 50 °C for about 1 h to obtain a solid PTX/copolymer matrix. Residual acetonitrile remaining in the film was removed under vacuum overnight at room temperature. The resultant thin film was hydrated with 4-ml water at 60 °C for 30 min to obtain a micelle solution, which was then filtrated through 0.2-μm filter membrane to remove the unincorporated PTX aggregates, followed by lyophilization. RITC-labeled Pluronic P123/F127 mixed polymeric micelles (RITC-PF) were also prepared by the method described above except that Pluronic P123 was substituted by a mixture of 10 wt.% RITC-labeled P123 and 90 wt.% P123. The RP-HPLC analysis of PTX in vitro was achieved on a C18 Gemini column (5 μm, 150 × 4.6 mm, Phenomenex, California, USA) with a mobile phase consisting of acetonitrile and ammonium acetate buffer solution (10 mM, pH 5.0) (50:45, v/v) at a flow rate of 1.0 ml/min. The effluents were monitored at 230 nm and quantified by comparing the peak areas with the standard curve.

Drug-loading coefficient (DL%) and encapsulation ratio (ER%) were calculated by the following equations. Polymeric mixed micelles were characterized on a Malvern Zetasizer Naso ZS (Malvern, UK) and by transmission electron microscopy (TEM) on a Philips CM 120 instrument. In order to create pseudo-sink condition, the in vitro release behavior of PTX from PF-PTX was monitored in PBS (pH 7.4) with 0.2% Tween-80 by dialysis method. One milliliter of PF-PTX (containing 0.1 mg PTX) was introduced into a dialysis bag (MWCO = 5000 Da, Greenbird Inc., Shanghai, China), and the end-sealed dialysis bag was submerged fully into 40 ml of PBS (pH 7.4) with 0.2% Tween-80 at 37 °C with stirring at 100 rpm for 96 h. At appropriate time intervals (0, 1, 4, 8, 12, 24, 48, 72 and 92 h), 0.5-ml aliquots were withdrawn and replaced with an equal volume of fresh medium. The concentration of PTX in samples was extracted with acetonitrile and determined by HPLC as described above with correction for the volume replacement.

$$\mathrm{DL}\% = \frac{\text{weight of the drug in micelles}}{\text{weight of the feeding polymer and drug}} \times 100\% \quad (1)$$

$$\mathrm{ER}\% = \frac{\text{weight of the drug in micelles}}{\text{weight of the feeding drug}} \times 100\% \quad (2)$$

2.4. Cellular accumulation of Rhodamine-123 and PTX

Cellular uptake of Rhodamine-123 (R-123) and PTX was determined in the presence or absence of known various concentrations

of blank Pluronic P123/F127 mixed micelles or unimers (PF) ranging from 0.001% to 1%. Cyclosporine A (CsA) was used as positive control and the inhibition concentration was 5 μM. A-549 cells were seeded in 24-well plates at densities of approximately 1×10^5 per well and grown until they reached 90–95% confluence. Solutions of 5 μM R-123 or 0.5 μg/ml PTX in RPMI 1640 medium with various concentrations of PF or CsA were equilibrated for a minimum of 1 h at 37 °C before use. The cells were washed with ice-cold PBS (pH 7.4) twice and allowed to equilibrate in RPMI 1640 for 30 min at 37 °C. Then, the medium was removed and cells treated with the treatment solutions. After 90 min of incubation, the supernatant was removed, and cells were washed with ice-cold PBS to remove all the traces of R-123 or PTX on the cell surface. In addition, in order to evaluate the kinetics of R-123 and PTX accumulation, cells were exposed to solutions of the mixed micelles (0.01%) containing 5 μM R-123 or 0.5 μg/ml PTX. At predetermined time intervals, experiments were conducted as described above. In the case of R-123, cells were lysed with PBS containing 1% Triton X-100 and centrifuged at 6000*g* for 6 min. R-123 concentrations in supernatants were measured using a fluorescence microplate reader (Tecan Safire2, Switzerland). As for PTX, the sample treatment was performed as reported earlier with minor modification [37–39]. Briefly, cells were lysed with 0.4 ml PBS containing 1% Triton X-100. After incubation, 100 μl cell lysate was withdrawn and extracted with methanol (200 μl/sample), and the mixture was then subjected to probe-type ultrasonic treatment (400 W, 10 cycles with 2 s active-3 s duration, JY92-II, Scientz Biotechnology Co., Ltd., China) in ice bath for further PTX extraction. The extracts were centrifuged at 6000*g* for 6 min, and the supernatants were subjected to HPLC analysis as described above. Cellular accumulation of R-123 and PTX was normalized with respect to total protein content. The protein content was determined using the BCA protein assay kit in accordance with the method specified by the manufacturer.

2.5. Determination of intracellular ATP

Cells were seeded in 12-well plates at a density of 2×10^5 per well and incubated overnight. Various concentrations of Pluronic empty mixed micelles or unimers (PF) in RPMI 1640 medium were added to cells and incubated at 37 °C for 2 h. 0.01% Pluronic P85 and FBS-free RPMI 1640 were used as positive and negative controls, respectively. After treatment, the cells were washed twice with ice-cold PBS and lysed with PBS containing 1.0% Triton X-100 at 37 °C for 30 min. Then, intracellular ATP was determined using ATP assay kit based on luciferin/luciferase assay and normalized for protein content. Light emission was measured with Ultra-Weak Luminescence Analyzer (model BPCL, Institute of Biophysics Academia Sinica, Beijing, China). Raw data were collected as relative light units integrated over 20 s for samples and converted to ATP concentrations with the aid of a standard calibration curve obtained using ATP standards.

2.6. Mitochondrial transmembrane potential measurement

Cells were seeded in 12-well plates at a density of 2×10^5 per well and incubated overnight. Various concentrations of PF in RPMI 1640 medium were added to cells and incubated at 37 °C for 2 h. After washing, mitochondrial transmembrane potential ($\Delta\Psi$) was detected using the JC-1 mitochondrial membrane potential assay kit. To measure the mitochondrial transmembrane potential, 0.01% Pluronic P85 and FBS-free RPMI 1640 were used as positive and negative controls, respectively. Mitochondrial transmembrane potential ($\Delta\Psi$) was expressed as follows:

$$\Delta\Psi = (\text{JC-1 red/green})_{\text{treatment}} / (\text{JC-1 red/green})_{\text{nontreatment}} \times 100\% \quad (3)$$

2.7. Subcellular localization of RITC-PF

For this study, Pluronic P123 was labeled with rhodamine B isothiocyanate (RITC) as described above. A-549 cells grown on 14-mm^2 glass coverslips that were placed in 6-well plates were incubated with 0.1% RITC-PF in FBS-free RPMI 1640 medium for 2 h at 37 °C followed by treatment with organelle-selective dyes. Cells were incubated with 50 nM MitoTracker Green (30 min) and 10 μM Hoechst 33342 (10 min) to visualize mitochondria and nuclei, respectively. Then, the loading solution was removed, the cell monolayers were washed three times with ice-cold PBS and examined by confocal laser scanning microscopy (Leica TCS SP2, Germany).

2.8. In vitro cytotoxicity assay

Cells were seeded in 96-well plates at the density of 5×10^3 cells per well. After 24 h of incubation at 37 °C with 5% CO_2, the old growth medium was removed, and the cells were incubated for 24 h, 48 h and 72 h in the media containing either PTX formulations—PF-PTX and Taxol injection with various concentration or different excipients—Pluronic P85, P123, F127, Cremophor EL and blank mixed micelles with concentration ranging from 10 to 1000 μg/ml. Cell survival was then measured using tetrazolium salt MTT assay. Then, 180 μl of fresh growth medium and 20 μl of MTT (5 mg/ml) solution were added to each well. The plate was incubated for an additional 4 h, and then 200 μl of DMSO was added to each well to dissolve any purple formazan crystals formed. The plates were vigorously shaken before taking measurement of relative color intensity. The absorbance at 570 nm of each well was measured by a microplate reader (Tecan Safire2, Switzerland).

2.9. Cell apoptosis

The cell apoptosis was first detected by assessment of nuclear morphology staining with Hoechst 33342. Briefly, A-549 cells were seeded in 6-well plates containing a coverslip with 5×10^5 cells per well and cultured at 37 °C for 24 h. Cells were then incubated for another 24 h with Taxol, PF-PTX (PTX concentration of 0.1 μg/ml) and culture medium as control. Samples were then fixed with 4% paraformaldehyde in PBS (pH 7.4) at room temperature for 15 min, stained with 10 μg/ml Hoechst 33342 in PBS at room temperature for 15 min and washed twice with ice-cold PBS. Coverslips were mounted onto glass slide which were then examined under the fluorescent microscope (OLYMPUS, IX 71, Japan) and documented by photography. For the quantitative analysis of apoptosis, cells were left untreated or were treated with Taxol or PF-PTX for 24 h with drug (0.1 μg/ml). At the completion of treatment, non-adherent and adherent cells were trypsinized, centrifuged at 1000*g* for 5 min, washed three times with ice-cold PBS and resuspended in 200 μl of binding buffer. Thereafter, 5 μl of Annexin V-FITC and 10 μl of PI were added and mixed for 15 min in the dark. The stained cells were analyzed using a flow cytometer (FACSCalibur, BD, USA). Data analysis was performed using CellQuest software (Becton Dickinson, USA).

2.10. Cell cycle analysis

A-549 cells seeded on the 6-well plates were treated with Taxol and PF-PTX (PTX concentration of 0.1 μg/ml) at 37 °C for 4 to 24 h. Cells treated with culture medium served as control. At various time intervals, adherent and non-adherent cells were recovered. Cells (1×10^6) were collected by centrifugation, washed twice with ice-cold PBS and then fixed with 70% cold ethanol and stored at 4 °C for 24 h. Cells were centrifuged again, washed with cold PBS

twice, incubated with RNase A (0.1 mg/ml) for 1 h at 37 °C and stained with PI (0.1 mg/ml) for 30 min in the dark. The DNA content was measured by flow cytometry (FACSCalibur, BD, USA), and the percentage of cells in each phase of the cell cycle was evaluated using the ModFit software.

2.11. Pharmacokinetic and biodistribution

Twelve Sprague–Dawley (SD) rats were randomly assigned to two groups for pharmacokinetic investigation. Groups 1 and 2 received an i.v. injection of Taxol or PF-PTX through the tail vein, respectively at an equivalent dose of 6 mg/kg PTX *versus* the body weight. At time points of 0 (pre-dose), 5, 15, 30 min, 1, 2, 4, 6, 8, 10, 12 and 24-h post injection, 0.5 ml of blood was collected into heparinized polyethylene tubes via the femoral artery and centrifuged at 1000*g* for 10 min to obtain plasma. The plasma was stored at −70 °C prior for analysis by HPLC. To examine the biodistribution of PF-PTX and Taxol, 80 Kunming strain mice were divided into two groups at random and given a single 6 mg/kg dose of PTX by the tail vein injection. At 5, 15, 30 min, 1, 2, 4, 6, 8, 10 and 12 h after injection, four mice in one group were sacrificed by cervical dislocation after drawing blood from the eyeball. Following closely, the blood was immediately treated as described above. The organs of heart, liver, spleen, lung and kidney were excised and thoroughly washed with ice-cold saline, then blotted dry, weighted and stored at −70 °C until assessed for PTX concentration by HPLC. The tissues were homogenized in a mixed solution of acetonitrile and water (50:50, v/v) before extraction.

Liquid–liquid extraction was performed prior to analysis. Briefly, 200-μl samples of plasma or tissues were mixed with 3 ml of diethyl ether containing 50 μl of 1.0 μg/ml diazepam as an internal standard. The samples were extracted on vortex-mixer for 2 min and then centrifuged at 6000*g* for 10 min. Next, the organic layer was transferred to a clean tube and evaporated under a gentle stream of nitrogen. The extraction residue was reconstituted in 100-μl acetonitrile and centrifuged at 1500*g* for 5 min before HPLC analysis. BAPP 2.0 (Bioavailability program package 2.0, 2002, China) was utilized to analyze the pharmacokinetic parameters such as the area under the plasma concentration–time curve (AUC), the apparent volume of distribution (V_d), total body clearance (CL), elimination half-life ($t_{1/2\beta}$) and mean residence time (MRT) of PTX for each formulation. The Akaike's information criterion (AIC) rule was observed in the determination of the appropriate compartment model.

2.12. In vivo antitumor efficacy

The therapeutic effect of PF-PTX was estimated using male BALB/c nude mice model (5–6 weeks, 18–22 g), which was inoculated subcutaneously with 5×10^6 A-549 human lung cancer cell line. When the tumor volume reached about 50–100 mm^3, mice were randomly assigned to three groups ($n = 6$): group 1 for saline solution, group 2 for Taxol injection (10 mg/kg) and group 3 for PF-PTX (10 mg/kg), respectively. Mice were administrated injection through the tail vein every 4 days for three times. The tumor diameters were measured every other day with a vernier caliper in two dimensions. Individual tumor volume (V) was calculated using the formula: $V = (L \times W^2)/2$, wherein length (L) is the longest diameter and width (W) is the shortest diameter perpendicular to length. In addition, for safety evaluation of the control and PTX formulations, the body weight of each mouse was determined every alternate day. At the end of the experiment, the animals were sacrificed by cervical dislocation, and the tumor mass was harvested, photographed and weighted. Last, the liver tissue was processed routinely into paraffin, sectioned at a thickness of 5 μm and stained with hematoxylin and eosin (H&E) for histopathological analysis.

2.13. Statistical analysis

Statistical analysis was performed by Student's *t*-test for two groups and one-way ANOVA for multiple groups. All results were expressed as the mean ± standard deviation (SD). A probability (p) of less than 0.05 is considered statistically significant.

3. Results and discussion

3.1. Preparation and characterization of PF-PTX polymeric micelles

The DL% and ER% calculated by Eqs. (1) and (2) were 1.39 ± 0.04% and 95.09 ± 2.91%, respectively. The blank micelles obtained were close to 20 nm, with an acceptably good polydispersity index (PDI) between 0.09 and 0.12, and the surface charge was −4.17 ± 0.78 mV. Upon loading with PTX, the mean diameter and surface charge remained at 21.34 ± 1.99 nm (Fig. 2A) and

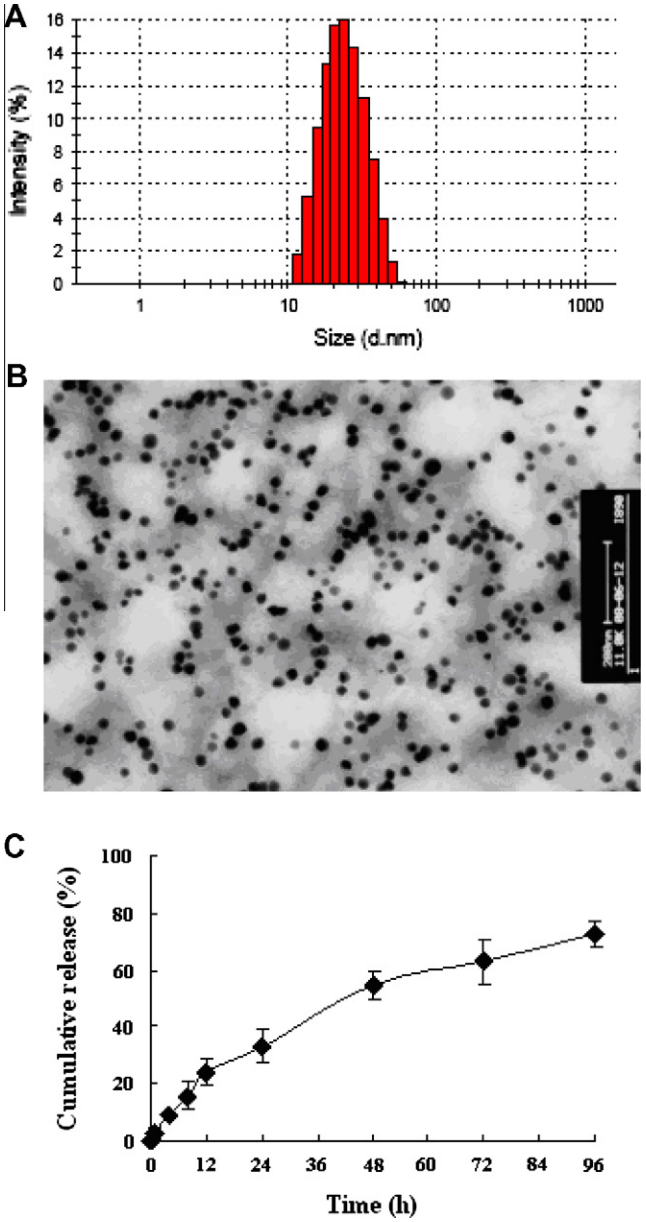

Fig. 2. (A) Micelle size and size distribution and (B) TEM image of PF-PTX. (C) Release profile of PF-PTX in PBS with 0.2% Tween-80 at 37 °C. Each point represents mean ± SD ($n = 3$). (For interpretation of the references to colour in this figure legend, the reader is referred to the web version of this article.)

−4.43 ± 1.17 mV, respectively. Lack of change in particle size and ζ potential were indicative that the drug was distributed in the hydrophobic micelle core rather than adsorbed to the surface of polymeric micelles [16,40]. As seen from Fig. 2B, PF-PTX exhibited spherical shape of moderate uniform particle size, and the particle size measured from the TEM image was in good agreement with that measured by the laser scattering technique. Furthermore, the ~20 nm diameter of polymeric micelles is below the pore size of the permeable vasculature found in many solid tumors, suggesting that PF-PTX should be able to selectively accumulate in solid tumors by means of the enhanced permeability and retention (EPR) effect. The in vitro release profile of PF-PTX shown in Fig. 2C indicated that nearly 75% of PTX was released within 4 days. This result showed that the micelle carrier can not only solubilize the poorly soluble drugs, but also sustain PTX release. The release profiles of polymeric micelles were fitted with four different model equations, including zero kinetics, first kinetics, Higuchi and Ritger–Peppas equations. The highest correlation coefficient indicated the best-fit release kinetics. The results showed that PTX release from PF-PTX was best fitted with the first kinetics ($r = 0.9985$) in PBS (pH 7.4) with 0.2% Tween-80.

3.2. Cellular accumulation of Rhodamine-123 and PTX

To evaluate the effects of the PF on MDR transporters-mediated efflux, the accumulation of R-123 and PTX was examined in A-549 cell line. As shown in Fig. 3A and B, following 90-min incubation, both R-123 and PTX showed an increase in accumulation with increasing concentrations of PF followed by a decline in their accumulation. Furthermore, the accumulation was greater than or equal to the standard P-gp inhibitor CsA over a wide range of concentrations of PF (0.001–0.1%). Interestingly, accumulation of R-123 and PTX was all reached a maximum at 0.01% block polymer concentration, which was close to the CMC value of mixed micelles (0.0059%) [35]. In other words, the enhancement in accumulation began below the CMC and increased up to a critical concentration near the CMC of the mixed micelles, which was also in agreement with the previous studies reported by Batarkova et al. [41]. Additionally, the reduction in drug in accumulation at higher concentrations (>0.1%) of the block copolymer could be attributed to partitioning of the drug into micelles that decreased the free drug concentration available for uptake [42,43]. However, it was also reported recently that above the CMC, although micellar trapping could contribute to decreased accumulation, inhibition of P-gp was not affected [44]. Noteworthy, it is well known that above the CMC, the concentration of unimers remains constant with any further increase in Pluronic copolymers resulting in the formation of micelles that are in dynamic equilibrium with the unimers. Since the concentration of unimers is constant above the CMC, the ability of Pluronic micelles to modulate MDR would not be diminished at concentrations above the CMC. Therefore, it is possible that the PF-PTX system can result in not only passive targeting to the tumor tissue through the enhanced permeability and retention (EPR) effect, but also modulation of drug resistance in MDR tumor cells by Pluronic block copolymers. Additionally, the time dependence of drug accumulation was assessed over 3 h with or without block copolymers at peak effect concentrations (Fig. 3C and D). It was shown that there were a large and rapid increase in R-123 and PTX accumulation compared to R-123 and PTX alone over the first 60 min, which then increased at a slower rate within the rest time. Furthermore, for NCI/ADR-RES cell, a breast MDR tumor cell overexpressed with P-gp, the R-123 and PTX accumulation situation was found to be similar to that of A-549 (data not shown). Thus, although whether Pluronic copolymers can modulate LRP is still not clear, the results described above suggested that PF could effectively enhance drug accumulation in MDR lung tumor cell line A-549.

3.3. Effects of PF on intracellular ATP and mitochondrial potential

To further understand the mechanisms by which Pluronic blank mixed micelles or unimers (PF) inhibited MDR, intracellular ATP and mitochondrial membrane potential ($\Delta\Psi$) levels were mea-

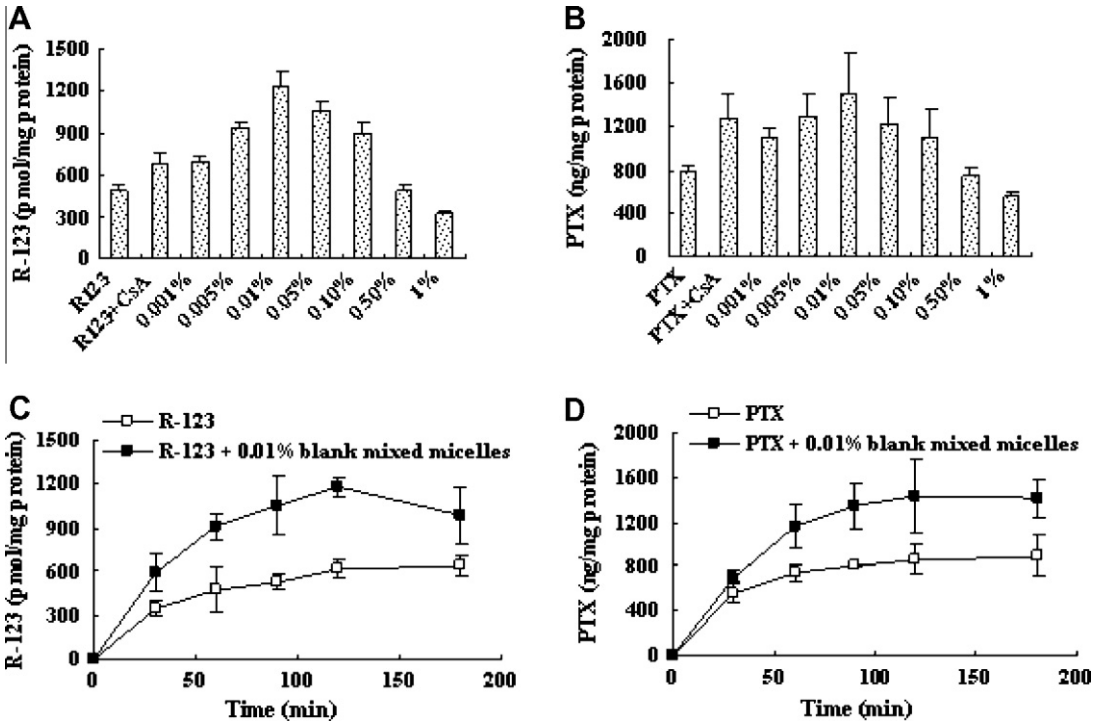

Fig. 3. Effect of blank Pluronic P123 and F127 mixed micelles or unimers (PF) on cellular accumulation of (A) R-123 and (B) PTX at 37 °C for 90 min. The time-dependent accumulation of (C) R-123 and (D) PTX in the presence of 0.01% blank mixed micelles in A-549 cells. Each point represents mean ± SD ($n = 3$).

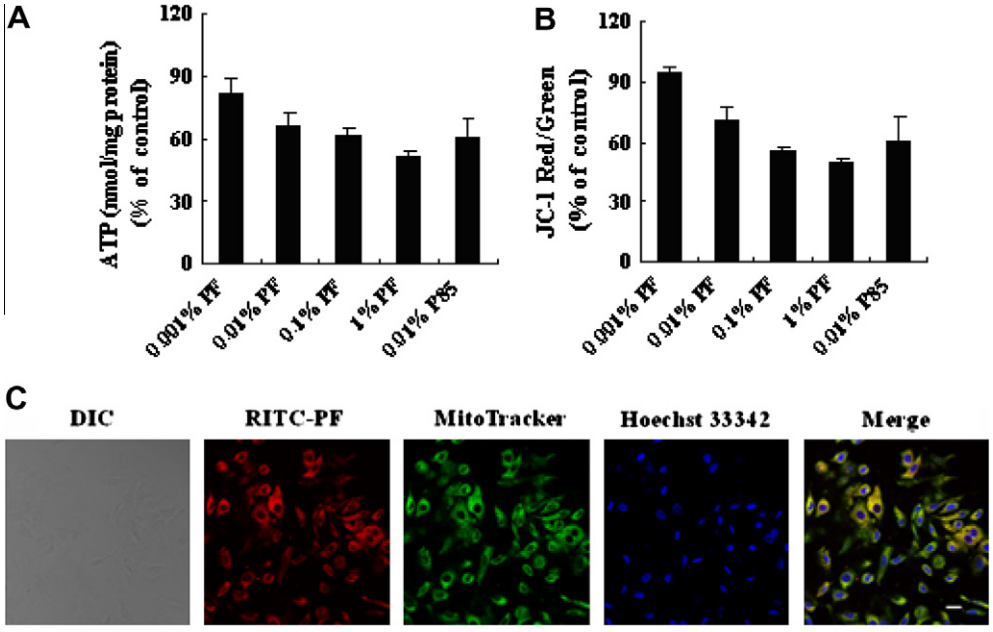

Fig. 4. The effects of Pluronic blank mixed micelles or unimers (PF) on intracellular ATP level (A) and mitochondrial transmembrane potential (B) in A-549 cells. Mitochondrial potential detection was based on the ratio of red fluorescence caused by the accumulation of JC-1 in mitochondrial and green fluorescence caused by the accumulation of JC-1 in cytoplasm. Each point represents mean ± SD ($n = 3$). (C) The confocal microscopy images showing the intracellular localization of RITC-PF in A-549 cells. The cells were exposed to 0.1% of RITC-PF for 2 h, washed with PBS and stained with 100 nM MitoTracker Green. Scale bar = 10 μm. (For interpretation of the references to colour in this figure legend, the reader is referred to the web version of this article.)

sured after exposure to various concentrations of PF. As shown in Fig. 4A and B, in A-549 tumor cells, it appeared that ATP and $\Delta\Psi$ levels all decreased in a concentration-dependent manner after treatment with PF. Over all tested concentrations (0.001–1%) of PF, ATP levels decreased from 81.52 ± 7.74% to 52.25 ± 2.15%, while $\Delta\Psi$ levels decreased from 94.26 ± 3.16% to 50.00 ± 1.91%. And the change of 0.01% PF in ATP and $\Delta\Psi$ was comparable to that of 0.01% Pluronic P85. Compared to control group, a significant effect on energy depletion and $\Delta\Psi$ was observed at 0.01% or higher concentrations of PF. Furthermore, after RITC-PF treatment, most of the RITC-PF was localized to mitochondria, as evidenced by colocalization of red fluorescence with that from MitoTracker Green (Fig. 4C). In this respect, indications that RITC-PF can reach and affect mitochondria in A-549 cells become crucial, because majority of proapoptotic stimuli including anti-cancer drugs require a mitochondrion-dependent step that involves permeabilization of the outer mitochondrial membrane and the release of mitochondrial proteins [45,46]. In addition, the loss of $\Delta\Psi$ is a hallmark for apoptosis. Apoptosis is a cellular process involving a genetically programmed series of events leading to the death of a cell. During this process, several key events occur in mitochondria, including loss of $\Delta\Psi$, changes in electron transport and the release of caspase activators such as cytochrome c. For this reason, $\Delta\Psi$ is an important parameter of mitochondrial function and has been used as an indicator of cell health [47]. It is also well known that mitochondria are ATP factory in cells and also are responsible for regulating apoptosis by releasing cytochrome *c* [47–49]. It appeared that there might be some additional mechanisms for modulation of MDR in A-549 cells besides ATP depletion. Thus, the exact molecular mechanism of action of PF needs to be further elucidated.

3.4. In vitro cytotoxicity assay

In vitro biocompatibility study of Pluronic P85, P123, F127, Cremophor EL and empty mixed micelles was carried out using A-549 cell line. In the concentration ranges ($\leqslant$10 μg/ml) used in this study, the cytotoxic effects of Pluronic F127, blank mixed micelles and Cremophor EL were negligible, as shown in Fig. 5A, C and E. However, it was shown that Pluronic P85, P123 and blank mixed micelles displayed increasing cytotoxicity as the concentration and incubation time increased, and this effect might be partly due to the cytostatic action of Pluronics. Rapoport et al. demonstrated that even 48-h incubation with Pluronic P105 micelles did not kill the A-2780 ovarian carcinoma cells but effectively prevented cell proliferation [50]. Additionally, it was shown by others that the cytotoxic effect of Pluronic unimers and micelles on non-cancerous cells was significantly lower than that on cancerous cells [50,51]. Although the growth inhibition of blank micelles against A-549 cells was significant (35.63 ± 2.74% of cell viability) at 1 mg/ml after 72 h of incubation, Cremophor EL exhibited much higher cytotoxicity than blank micelles at identical concentration. The viable A-549 cells after 3 days exposure with Cremophor EL were 18.68 ± 1.89%. As reported previously, Cremophor EL was significantly cytotoxic at concentration above 1 mg/ml [52,53]. In addition, the in vitro cytotoxicity of PF-PTX was investigated and compared with that of Taxol injection using A-549 cells (Fig. 5B, D and F). After 24 h, the cell viability was more inhibited by PF-PTX than by Taxol at all concentrations of PTX. The IC50 values at 24 h of Taxol and PF-PTX were 5.79 ± 1.37 and 1.60 ± 0.69 μg/ml, respectively ($p < 0.05$). Instead after 72-h treatment, the IC_{50} values of Taxol and PF-PTX decreased to 0.36 ± 0.17 and 0.059 ± 0.012 μg/ml, respectively ($p < 0.05$). It was straightforward to understand that both incubation time and concentration played a major role in the in vitro cytotoxicity of PTX, viz. higher drug concentration and longer incubation time would cause lower cell viability. For longer incubation, periods a larger number of cells could enter the G_2/M phase during which PTX was more active [54]. Furthermore, the in vitro cytotoxicity studies suggested that Pluronic may act as a chemosensitizer and potentiate cytotoxic effects of PTX in A-549 lung MDR tumor cell, partly due to the selective energy-depleting effects of Pluronic copolymers, which was in close agreement with the results reported by Batrakova et al. [55].

3.5. Cell apoptosis

To examine whether the encapsulation of PTX in mixed micelles modifies cell apoptosis, we used the Hoechst 33342 staining method to provide evidence for the PTX-induced apoptotic cell death. The nuclei of untreated A-549 cells showed homogenous fluorescence with no evidence of segmentation and fragmentation after Hoechst 33342 staining. In contrast, segregation of the cell nuclei into segments, indicating possible DNA condensation, became apparent in the cells after 24 h of incubation with Taxol as presented in Fig. 6A. Nuclear integrity was, however, relatively intact in these cells. On the other hand, the cell nuclei became severely fragmented when the cells were treated for 24 h with PF-PTX, suggesting the nuclei were segmentated into dense nuclear parts and further distributed into apoptotic bodies. To measure the apoptotic effect of Taxol and PF-PTX quantitatively, A-549 cell apoptosis was evaluated, and the percentage of cell apoptosis treated with Taxol and PF-PTX was determined by flow cytometer as shown in Fig. 6B. Annexin V is a 35–36 kDa Ca^{2+}-dependent phospholipid-binding protein that has a high affinity for membrane phospholipid phosphatidylserine, which is translocated from the inner to the outer leaflet of the plasma membrane in cell apoptosis. PI is a standard

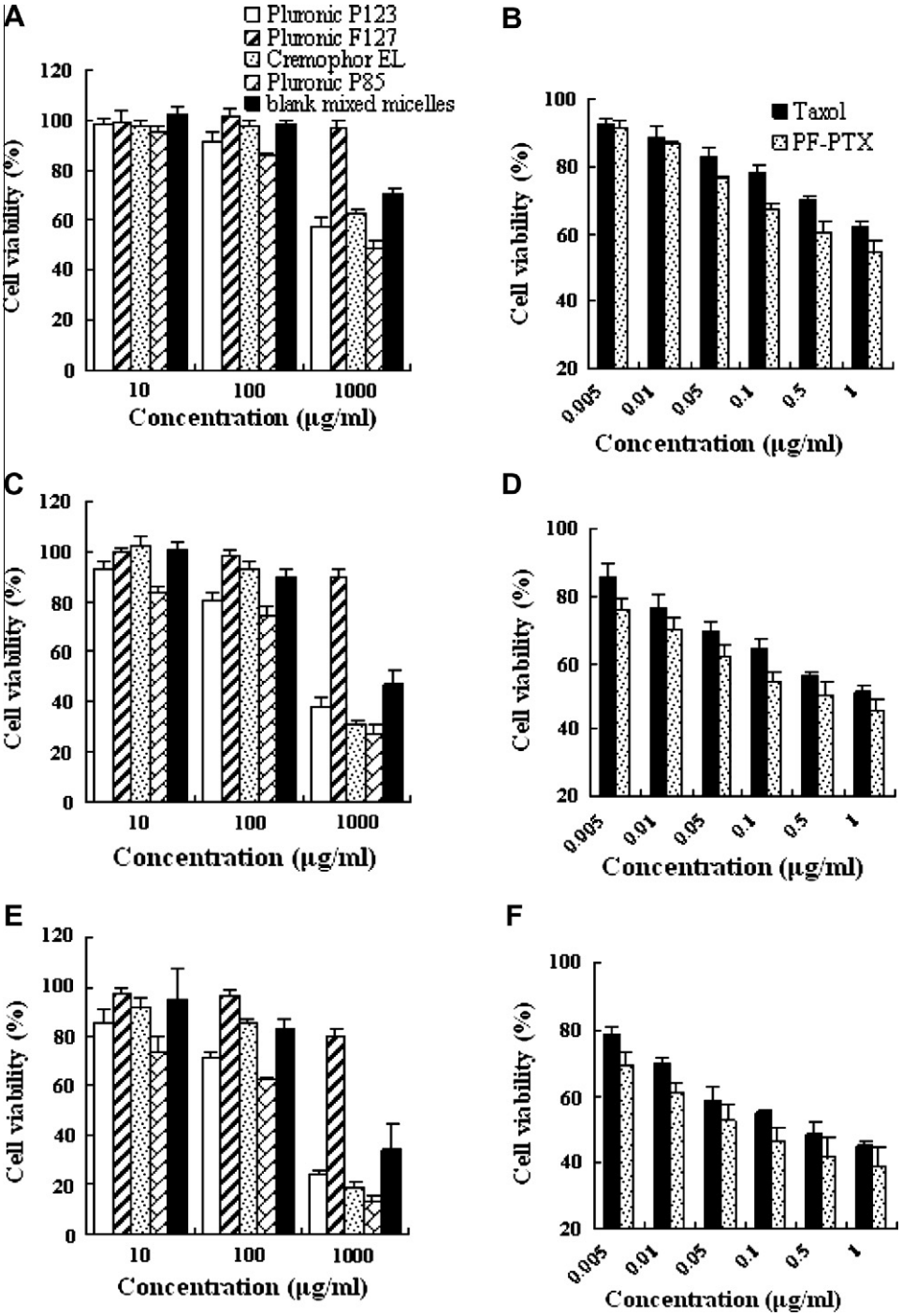

Fig. 5. Viability of A-549 cells as a function of varying concentrations of excipients (Pluronic P85, P123, F127, Cremophor EL and blank mixed micelles) at day 1 (A), day 2 (C) and day 3 (E); In vitro cytotoxicy of Taxol and PF-PTX at various concentrations of PTX against A-549 cells at day 1 (B), day 2 (D) and day 3 (F). Each point represents mean ± SD (n = 3).

flow cytometric viability molecular probe and is used to distinguish viable from nonviable cells. Viable cells with intact membranes exclude PI, whereas the membranes of dead and damaged cells are permeable to PI. Thus, Annexin V-FITC staining in conjunction with PI can distinguish early apoptosis from late apoptosis or living cells from necrotic cells. The percentage of early and late apoptosis of Taxol-treated A-549 cells was 5.67 ± 1.89% and 13.60 ± 2.11%, respectively, while PF-PTX caused 4.90 ± 0.37% and 21.26 ± 2.73% of both early and late cell apoptosis, which was consistent with the observed results of cellular nulceus staining and in vitro cytotoxicity and indicated that PF-PTX induced more late apoptosis due to more uptake of PTX and produced higher cytotoxicity than Taxol. This effect may be attributed to the inhibition of the most clinically relevant drug efflux transporters and the significant regulation of the intracellular levels of antiapoptotic and proapoptotic genes in MDR tumor cells by Pluronic block copolymers [56–59].

3.6. Cell cycle analysis

It has been reported that PTX could impair mitosis and induce cell cycle arrest [54]. Drug-induced G_2/M arrest is associated with double-strain DNA breakage and extensive chromosome damage [60]. Therefore, the increased G_2/M phase arrest indicates cell division inhibition and cell growth restrain [61]. In this study, Taxol and PF-PTX were investigated to determine whether they could induce the cell cycle arrest in A-549 cells. Distribution of the A-549 cells into the various phases of the cell cycle following the incubation of PTX formulations at different time points was shown in Fig. 7. It was obvious that when A-549 cells were treated with Taxol or PF-PTX with 0.1 μg/ml PTX, a reduction in the fraction of cell in the G_0/G_1 and S phase, and a higher accumulation of cells in the G_2/M phase were found with increasing incubation time. As for the percentage of the G_2/M phase, there was nearly no difference between Taxol and PF-PTX after 4-h incubation (16.62% and 19.01%, respectively), but it obviously increased from 8 to 24 h in PF-PTX group compared to Taxol. Quantitative analysis of the cell cycle distribution after 24-h incubation with PTX formulations revealed that only 11.40% of the cells were in the G_2/M phase for control cells, whereas the G_2/M populations for Taxol and PF-PTX were 65.94% and 81.23%, respectively. These data may suggest that the boosted cytotoxicity observed for PF-PTX was a result of enhanced intracellular PTX concentration. Thus, the results demonstrated that ATP depletion by PF played an important role in PTX-induced apoptosis and cell arrest in the G_2/M phase.

3.7. Pharmacokinetic and biodistribution

The pharmacokinetic of PF-PTX in comparison with that of Taxol after i.v. administration to SD rats at the same 6 mg/kg PTX dose was shown in Fig. 8A. We can see from this figure that the PF-PTX formulation achieved much larger AUC and much longer half-life compared to Taxol. The concentrations of PTX delivered by mixed micelles were higher than Taxol during all experimental hours. The PTX plasma concentration–time curves for both PF-PTX and Taxol were all fitted well with the two-compartment model. The pharmacokinetic parameters for PTX in plasma were estimated by compartmental method shown in Table 1. In the case of PF-PTX, the $AUC_{0\to\infty}$ was 14505.14 μg/L/h which was 2.2 times higher than that of Taxol. In addition, elimination half-life ($t_{1/2\beta}$) and MRT for the formulation of PF-PTX were 3.13-fold and 2.96-fold higher than Taxol, respectively. In contrast, CL for PF-PTX was significantly lower than that of Taxol implying a longer retention of the drug in blood circulation. Although Taxol can alter the biodistribution of PTX as a result of entrapment of the drug into the circulating Cremophor EL micelles [62,63], the pharmacokinetic results indi-

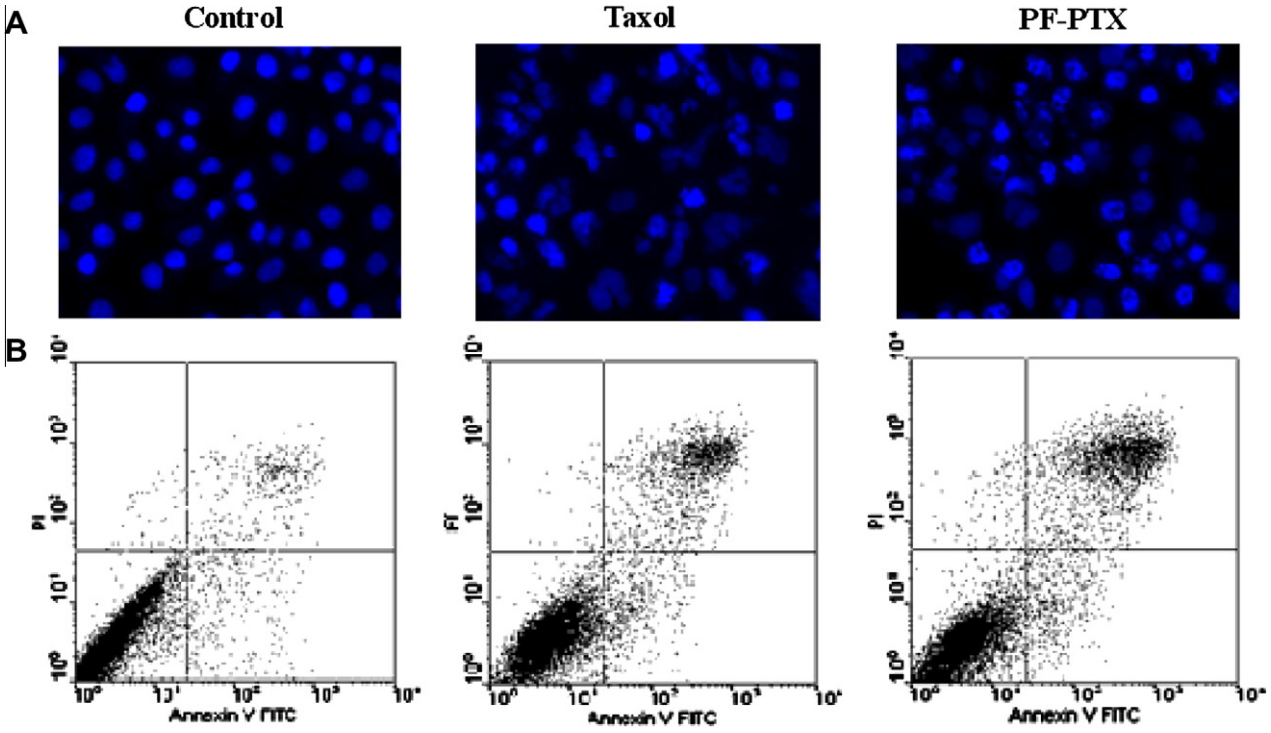

Fig. 6. Induction of apoptosis on A-549 human lung cancer cells by Taxol and PF-PTX. (A) Fluorescence micrographs at 40× magnification of A-549 cell nuclei following 24-h incubation with Taxol and PF-PTX at equivalent PTX concentration (0.1 μg/ml). (B) Cell apoptosis analysis of A-549 cells by flow cytometry using staining of Annexin V-FITC and PI. The cells that took up PI but did not bind Annexin V-FITC would most likely be necrotic were shown in the upper left quadrant; late apoptotic cells that bind Annexin V-FITC and PI in upper right quadrant; early apoptotic cells binding Annexin V-FITC in lower right quadrant; viable cells binding neither Annexin V-FITC nor PI in lower left quadrant. (For interpretation of the references to colour in this figure legend, the reader is referred to the web version of this article.)

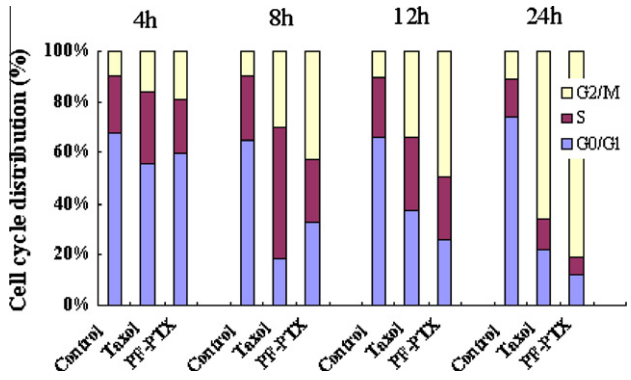

Fig. 7. The cell cycle distribution determined by FACS analysis and expressed by percentages. The experiment was performed in duplicate, and the values presented here are the mean of the two replicates. (For interpretation of the references to colour in this figure legend, the reader is referred to the web version of this article.)

cated that the PF-PTX formulation had longer systemic circulation time and slower plasma elimination rate than those of Taxol, which was in good agreement with the studies reported by Han and Wang [64,65]. The effect of PTX-loaded Pluronic P123 or P105 micelles all resulted in higher $t_{1/2\beta}$ (>2.3-fold) and $AUC_{0\rightarrow t}$ (>2.9-fold) than Taxol injection ($p < 0.01$). This long blood circulation may be attributed to the long hydrophilic shell of mixed micelles formed by PEO segments of Pluronic block copolymer that reduce the rate of mononuclear phagocyte system (MPS) uptake [66,67]. Therefore, these results illustrated the potential utility of Pluronic polymeric micelles as long circulating nanocarriers for poorly soluble anti-cancer drugs.

PTX concentrations investigated in blood and organs of heart, liver, spleen, lung and kidney after i.v. administration of PF-PTX and Taxol were presented in Fig. 8B. The total amount of drug accumulated in each organ within 12 h ($AUC_{0\rightarrow 12\ h}$) was calculated by trapezoidal rule, and the results were shown in Fig. 8B. The PTX concentrations in blood changed over time demonstrated the same trends revealed in pharmacokinetic studies. PTX was widely and rapidly distributed into most tissues following i.v. administration of Taxol injection. The $AUC_{0\rightarrow 12\ h}$ in these tissues for Taxol group was decreased in the following order: liver > spleen > lung > kidney > heart > plasma. In contrast, the corresponding order for PF-PTX was lung > liver > spleen > kidney > plasma > heart. The PTX $AUC_{0\rightarrow 12\ h}$ of PF-PTX was higher in plasma and lung, lower

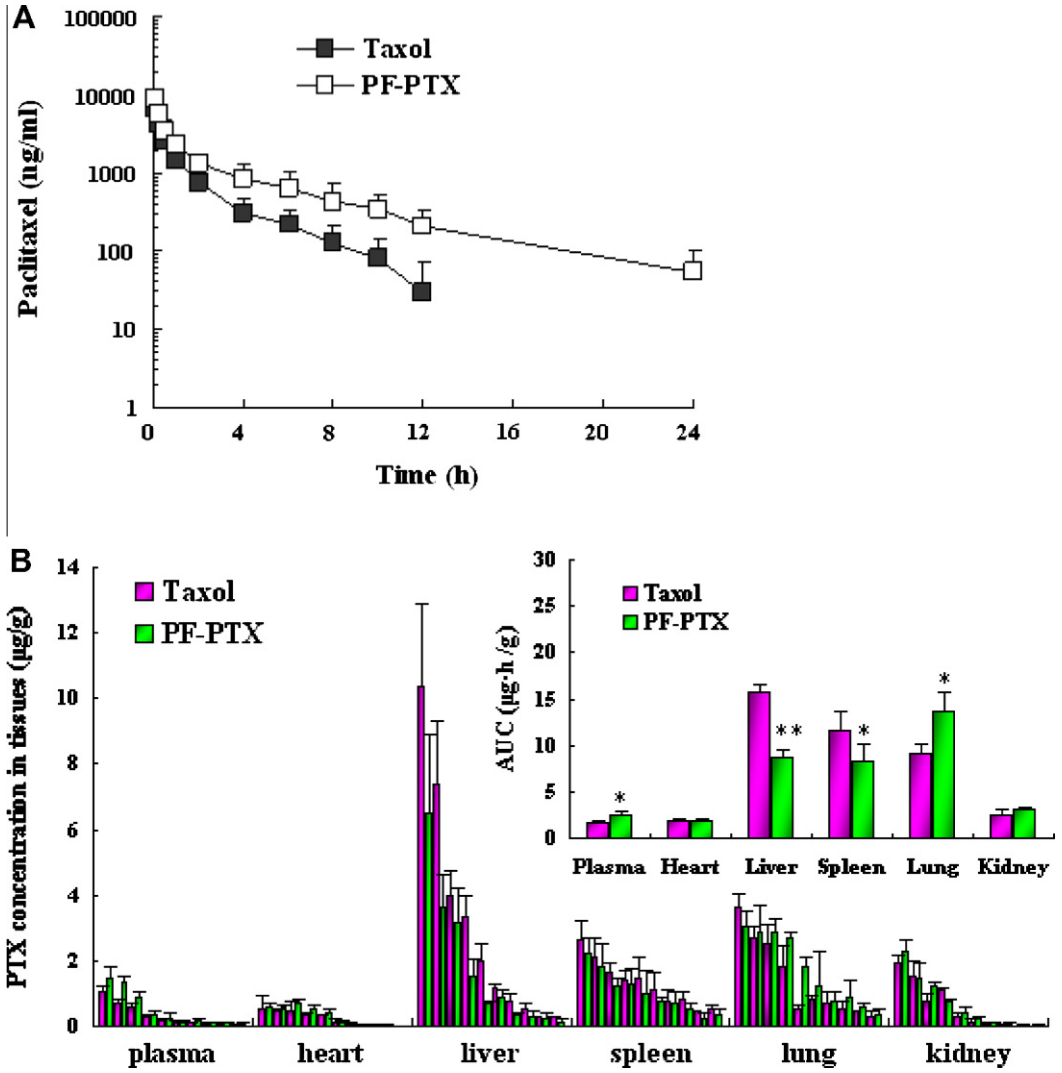

Fig. 8. (A) Plasma concentration–time curves of PF-PTX and Taxol after i.v. administration to SD rats at the same 6 mg/kg PTX dose (mean ± SD, $n = 6$). (B) The PTX concentration of PF-PTX and Taxol in tissues at different times following i.v. administration to KM mice at a single 6 mg/kg dose of PTX. Inset shows that comparative tissue distribution ($AUC_{0\rightarrow 12\ h}$) of PTX formulations (mean ± SD, $n = 4$). $^{*}p < 0.05$, $^{**}p < 0.01$, compared with Taxol. (For interpretation of the references to colour in this figure legend, the reader is referred to the web version of this article.)

Table 1
Comparative pharmacokinetic parameters of PTX formulations ($n = 6$).

Parameters	Formulations	
	Taxol	PF-PTX
$t_{1/2}(\alpha)$ (h)	0.91 ± 0.13	2.82 ± 1.71*
$t_{1/2}(\beta)$ (h)	2.64 ± 0.34	8.26 ± 5.32*
$AUC_{0\to t}$ (μg/L/h)	6330.58 ± 1773.51	13,370.82 ± 4758.70*
$AUC_{0\to\infty}$ (μg/L/h)	6603.57 ± 1894.07	14,505.14 ± 4448.11**
MRT (h)	2.37 ± 0.65	7.02 ± 2.61**
CL (L/h/kg)	1.00 ± 0.34	0.47 ± 0.17**
V_d (L/kg)	3.72 ± 0.96	5.96 ± 5.53

* $p < 0.05$.
** $p < 0.01$, compared with Taxol.

in liver and spleen compared to Taxol. There were significantly different concentrations in plasma, liver, spleen and lung between PF-PTX and Taxol ($p < 0.05$). Therefore, the PEO hydrophilic shell of PF-PTX efficiently decreased the adsorption of plasma protein to micelles, and greatly reduced the elimination by MPS and accumulation in the liver and spleen. Additionally, PTX concentrations of PF-PTX group in lung maintained a great higher level than those of Taxol as shown in Fig. 8B. This may be due to the distribution nature of Pluronic mixed micelles followed by a slow release of the drug [68,69]. Furthermore, it was reported that Pluronics could interact with the lung surfactant lipid monolayers (DPPC or cholesterol/DPPC monolayers) through hydrophobic interaction, van der Waals forces and hydrogen bonding effect [70], which probably induced aggregation of the mixed micelles in lung. Therefore, the PF-PTX was expected to be a potential drug delivery system of PTX for overcoming MDR in lung cancer.

3.8. In vivo antitumor efficacy

The average tumor growth rate in close comparison with those of the control (saline only) and the Taxol group was shown in Fig. 9A. We can see that the antitumor efficacy of PF-PTX was superior to that of all other treatments. For example, tumor growth in the PF-PTX group was inhibited to such an extent that, at 28 days, tumor volume in this group was only 31.8% that of the Taxol group. In other words, the PF-PTX formulation showed about three times more effective than Taxol in controlling tumor growth. By considering the overall slope of all the curves in Fig. 9A, it can be concluded that the PF-PTX had significant advantages over Taxol in suppressing A-549 solid tumors. The antitumor efficacy in vivo for PF-PTX and Taxol was consistent well with the cell experiment in vitro. Furthermore, from ANOVA with a confidence interval of 95%, most experimental data points obtained from the PF-PTX group after day 6 were found to be statistically significantly differ-

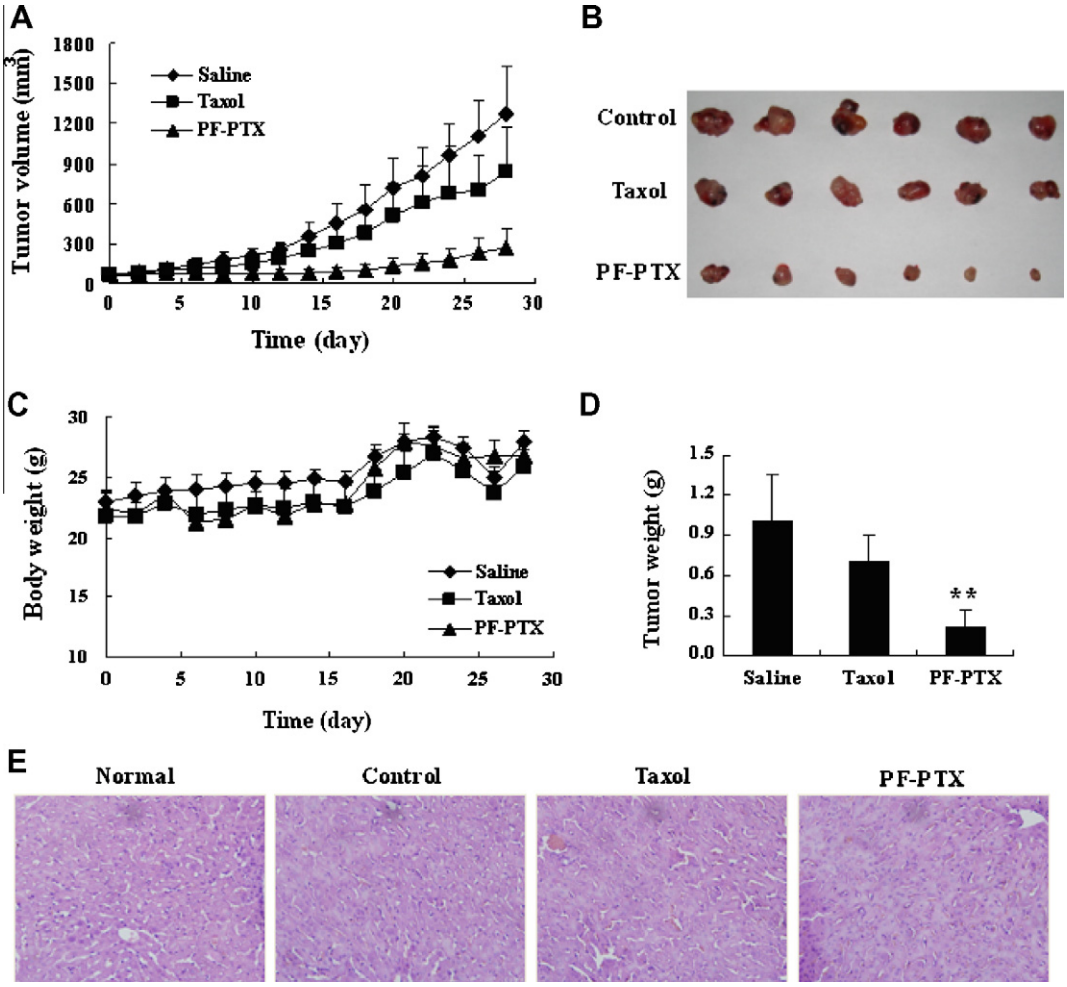

Fig. 9. (A) In vivo anti-cancer efficacy of different PTX formulations in A-549 tumor xenografts. (B) Photographs of tumors from each treatment group excised on day 28. (C) Change in body weight of animals as a function of time in subcutaneous A-549 xenograft-bearing male nude mice. (D) The weight of tumor mass of each treatment group at the time of sacrifice. (E) Liver sections isolated in the last day and stained with hematoxylin and eosin for histopathological analysis. Images were obtained under Olympus IX 71 fluorescence microscope using a 40× objective. *$p < 0.05$, **$p < 0.01$, compared with Taxol (mean ± SD, $n = 6$). (For interpretation of the references to colour in this figure legend, the reader is referred to the web version of this article.)

ent from those of Taxol injection. In addition, on the day of sacrifice, tumor mass was excised and photographed, as presented in Fig. 9B. The weights of excised tumor mass from the A-549 xonegraft model after treatments were shown in Fig. 9D. The untreated tumor weighted 1.00 ± 0.35 g, while the animals treated with Taxol and PF-PTX had tumor weights of 0.70 ± 0.20 g and 0.21 ± 0.12 g. Taken together, it was shown that the antitumor efficacy of PF-PTX formulation was greatly superior to that of Taxol injection in A-549 MDR tumor model. These results might be explained by the increased local concentration of PTX in the tumor tissue, since accumulation of PF-PTX in tumors was favored by their long circulation time and by EPR effect. Thus, PF-PTX appeared to retain the desirable effects of passive targeting because of the long PEO shell and also exhibit the drastic sensitization of MDR tumors conferred by Pluronic copolymers. Additionally, the change in body weight as a function of time in tumor-bearing animals was used as one of the marker of safety. As shown in Fig. 9C, the body weights of mice treated with PF-PTX and Taxol recovered after cessation of drug treatment. Neither complete tumor growth regression nor toxicity-induced death was observed in any experimental group. There was no serious body weight loss in mice treated with PF-PTX and Taxol, but the size of tumors treated by PF-PTX showed continuous reduction for 2 weeks after the i.v. injection. Furthermore, the liver tissue histology was done to determine cellular infiltration due to inflammatory response. There was no evidence of acute liver toxicity from either PF-PTX or Taxol therapy (Fig. 9E). However, intravenous administration of Taxol at the same dose of PF-PTX resulted in development of immediate ataxia, decreased activity and enhanced respiration which were reversed after a few minutes. These results implied that PF-PTX not only induced less systemic toxicity, but also inhibited MDR tumors, probably attributed to less random PTX release in the body while sustaining micellar integrity and the sensitization effect of multi-functional Pluronic copolymers.

4. Conclusions

In this study, we have investigated the potential for PF-PTX to enhance the antitumor efficacy in MDR human lung tumor cell line A-549. PF-PTX was able to effectively enhance the in vitro cytotoxicity and modify the cell apoptosis and cell cycle arrest compared to Taxol. In addition, the pharmacokinetic and biodistribution studies demonstrated that PF-PTX could significantly increase the blood circulation time of PTX. The therapeutic improvement of PF-PTX in vivo against MDR A-549 tumor was also obtained based on the synergistic effect of passive tumor targeting and MDR reversing ability of Pluronic copolymers. Taken together, PF-PTX seems to be a potential drug delivery system of PTX for lung MDR cancer chemotherapy.

Acknowledgments

We greatly acknowledged Prof. Jiandong Ding and Dr. Guangtao Chang for their help in polymer synthesis. We are grateful for the financial support from the National Basic Research Program of China 973 program (2007CB935802), National Natural Science Foundation of China (30873177) and National Science and Technology Major Project (2009ZX09310-006).

References

[1] A. Jemal, M.J. Thun, L.A. Ries, H.L. Howe, H.K. Weir, M.M. Center, Annual report to the nation on the status of cancer, 1975–2005, featuring trends in lung cancer, tobacco use, and tobacco control, J. Natl. Cancer Inst. 100 (2008) 1672–1694.
[2] A. Trussardi, G. Poitevin, M.C. Gorisse, M.J. Faroux, H. Bobichon, C. Delvincourt, J.C. Jardillier, Sequential overexpression of LRP and MRP but not P-gp 170 in VP16-selected A549 adenocarcinoma cells, Int. J. Oncol. 13 (1998) 543–548.
[3] W. Berger, U. Setinek, P. Hollaus, T. Zidek, E. Steiner, L. Elbling, H. Cantonati, J. Attems, A. Gsur, M. Micksche, Multidrug resistance markers P-glycoprotein, multidrug resistance protein 1, and lung resistance protein in non-small cell lung cancer: prognostic implications, J. Cancer. Res. Clin. Oncol. 131 (2005) 355–363.
[4] S. Meschini, M. Marra, A. Calcabrini, E. Monti, M. Gariboldi, E. Dolfini, G. Arancia, Role of the lung resistance-related protein (LRP) in the drug sensitivity of cultured tumor cells, Toxicol. in Vitro 16 (2002) 389–398.
[5] M. Kitazono, T. Sumizawa, Y.J. Takebayashi, Z.S. Chen, T. Furukawa, S.C. Nagayama, A. Tani, S. Takao, T. Aikou, S. Akiyama, Multidrug resistance and the lung resistance-related protein in human colon carcinoma SW-620 cells, J. Natl. Cancer Inst. 91 (1999) 1647–1653.
[6] H.K. Kang, E. Lee, H. Pyo, S.J. Lim, Cyclooxygenase-independent down-regulation of multidrug resistance-associated protein-1 expression by celecoxib in human lung cancer cells, Mol. Cancer Ther. 4 (2005) 1358–1363.
[7] Y. Imai, M. Nakane, K. Kage, S. Tsukahara, E. Ishikawa, T. Tsuruo, Y. Miki, Y. Sugimoto, C421A polymorphism in the human breast cancer resistance protein gene is associated with low expression of Q141K protein and low-level drug resistance, Mol. Cancer Ther. 1 (2002) 611–616.
[8] A. Hira, H. Watanabe, Y. Maeda, K. Yokoo, E. Sanematsu, J. Fujii, J. Sasaki, A. Hamada, H. Saito, Role of P-glycoprotein in accumulation and cytotoxicity of amrubicin and amrubicinol in MDR1 gene-transfected LLC-PK1 cells and human A549 lung adenocarcinoma cells, Biochem. Pharmacol. 75 (2008) 973–980.
[9] E. Lee, S.J. Lim, The association of increased lung resistance protein expression with acquired etoposide resistance in human H460 lung cancer cell lines, Arch. Pharm. Res. 29 (2006) 1018–1023.
[10] E.S. Lee, Z.G. Gao, D. Kim, K. Park, I.C. Kwon, Y.H. Bae, Super pH-sensitive multifunctional polymeric micelle for tumor pHe specific TAT exposure and multidrug resistance, J. Control. Release 129 (2008) 228–236.
[11] C.M. Spencer, D. Faulds, Paclitaxel – a review of its pharmacodynamic and pharmacokinetic properties and therapeutic potential in the treatment of cancer, Drugs 48 (1994) 794–847.
[12] A.K. Singla, A. Garg, D. Aggarwal, Paclitaxel and its formulation, Int. J. Pharm. 235 (2002) 179–192.
[13] R.B. Weiss, R.C. Donehower, P.H. Wiernik, Hypersensitivity reactions from Taxol, J. Clin. Oncol. 8 (1990) 1263–1268.
[14] J.H. Michael, S.S. Patrick, D. Neil, Protein nanoparticles as drug carrier in clinical medicine, Adv. Drug Deliv. Rev. 60 (2008) 876–885.
[15] K.S. Lee, H.C. Chung, S.A. Im, Y.H. Park, C.S. Kim, S.B. Kim, S.Y. Rha, M.Y. Lee, J. Ro, Multicenter phaseIItrial of Genexol-PM, a cremophor-free, polymeric micelle formulation of paclitaxel, in patients with metastatic breast cancer, Breast Cancer Res. Treat. 108 (2008) 241–250.
[16] H. Devalapally, Z. Duan, M.V. Seiden, M.M. Amiji, Modulation of drug resistance in ovarian adenocarcinoma by enhancing intracellular ceramide using tamoxifen-loaded biodegradable polymeric nanoparticles, Clin. Cancer Res. 14 (2008) 3193–3203.
[17] G. Bradley, P.F. Juranka, V. Ling, Mechanism of multidrug resistance, Biochem. Biophys. Acta. 948 (1988) 87–128.
[18] A.L. Harris, D. Hochhauser, Mechanisms of multidrug resistance in cancer treatment, Acta. Oncol. 31 (1992) 205–213.
[19] A. Rahman, S.R. Husain, J. Siddiqui, M. Verma, M. Agresit, M. Center, A.R. Safa, R.I. Glazer, Liposome-mediated modulation of multidrug resistance in human HL-60 leukemia cells, J. Natl. Cancer Inst. 84 (1992) 1909–1915.
[20] D.J. Booser, F.J. Esteva, E. Rivera, V. Valero, G.L. Esparza, W. Priebe, G.N. Hortobagyi, Phase II study of liposomal annamycin in the treatment of doxorubicin-resistant breast cancer, Cancer. Chemother. Pharmacol. 50 (2002) 6–8.
[21] E. Garcion, A. Lamprecht, B. Heurtault, A. Paillard, A. Aubert-Pouessel, B. Denizot, P. Menei, J.P. Benoit, A new generation of anticancer, drug-loaded, colloidal vectors reverses multidrug resistance in glioma and reduces tumor progression in rats, Mol. Cancer. Ther. 5 (2006) 1710–1722.
[22] C. Vauthier, C. Dubernet, C. Chauvierre, I. Brigger, P. Couvreur, Drug delivery to resistant tumors: the potential of poly (alkyl cyanoacrylate) nanoparticles, J. Control. Release 93 (2003) 151–160.
[23] J.M. Koziara, T.R. Whisman, M.T. Tseng, R.J. Mumper, In-vivo efficacy of novel paclitaxel nanoparticles in paclitaxel-resistant human colorectal tumors, J. Control. Release 112 (2006) 312–319.
[24] T. Minko, P. Kopeckova, V. Pozharov, J. Kopeck, HPMA copolymer bound adriamycin overcomes MDR1 gene encoded resistance in a human ovarian carcinoma cell line, J. Control. Release 54 (1998) 223–233.
[25] T. Minko, P. Kopeckova, J. Kopeck, Preliminary evaluation of caspases-dependent apoptosis signaling pathways of free and HPMA copolymer-bound doxorubicin in human ovarian carcinoma cells, J. Control. Release 71 (2001) 227–237.
[26] A.V. Kabanov, E.V. Batrakova, V.Y. Alakhov, Pluronic block copolymers for overcoming drug resistance in cancer, Adv. Drug Deliv. Rev. 54 (2002) 759–779.
[27] E.V. Batrakova, D.L. Kelly, S. Li, Y. Li, Z. Yang, L. Xiao, D.Y. Alakhova, S. Sherman, A.V. Kabanov, V.Y. Alakhov, Alteration of genomic responses to doxorubicin and prevention of MDR in breast cancer cells by a polymer excipient: Pluronic P85, Mol. Pharm. 3 (2006) 113–123.
[28] L.S. Jabr-Milance, L.E. van Vlerken, S. Yadav, M.M. Amiji, Multi-functional nanocarriers to overcome tumor drug resistance, Cancer Treat Rev. 34 (2008) 592–602.
[29] S. Danson, D. Ferry, V.Y. Alakhov, J. Margison, D. Kerr, D. Jowle, M. Brampton, G. Halbert, M. Ranson, Phase I dose escalation and pharmacokinetic study of

pluronic polymer-bound doxorubicin (SP1049C) in patients with advanced cancer, Br. J. Cancer 90 (2004) 2085–2091.
[30] Y. Matsumura, T. Hamaguchi, T. Ura, K. Muro, Y. Yamada, Y. Shimada, K. Shirao, T. Okusaka, H. Ueno, M. Ikeda, N. Watanabe, Phase I clinical trial and pharmacokinetic evaluation of NK911, a micelle-encapsulated doxorubicin, Brit. J. Cancer 91 (2004) 1775–1781.
[31] Y. Mizumura, Y. Matsumura, M. Yokoyama, T. Okano, T. Kawaguchi, F. Moriyasu, T. Kakizoe, Incorporation of the anticancer agent KRN5500 into polymeric micelles diminishes the pulmonary toxicity, Jpn. J. Cancer Res. 93 (2002) 1237–1243.
[32] Y. Matsumura, Preclinical and clinical studies of anticancer drug-incorporated polymeric micelles, J. Drug Target 15 (2007) 507–517.
[33] A. Armstrong, J. Brewer, C. Newman, V. Alakhov, G. Pietrzynski, S. Campbell, P. Corrie, M. Ranson, J.W. Valle, SP1049C as first-line therapy in advanced (inoperable or metastatic) adenocarcinoma of the oesophagus: a phaseIIwindow study. ASCO Annual Meeting Proceedings Part I, J. Clin. Oncol. 24 (2006) 4080.
[34] E.V. Batrakova, A.V. Kabanov, Pluronic block copolymers: Evolution of drug delivery concept from inert nanocarriers to biological response modifiers, J. Control. Release 130 (2008) 98–106.
[35] W. Zhang, J.G. Hao, Y. Shi, Y.J. Li, J. Wu, X.Y. Sha, X.L. Fang, Paclitaxel-loaded Pluronic P123/F127 mixed polymeric micelles: formulation, optimization and in vitro characterization, Int. J. Pharm. 376 (2009) 176–185.
[36] H.F. Lu, W.S. Lim, J. Wang, Z.Q. Tang, P.C. Zhang, K.W. Leong, S.M. Chia, H. Yu, H.Q. Mao, Galactosylated PVDF membrane promotes hepatocyte attachment and functional maintenance, Biomaterials 24 (2003) 4893–4903.
[37] Y.B. Patil, U.S. Toti, W. Wong, A. Khdair, L. Ma, J. Panyam, Single-step surface functionalization of polymeric nanoparticles for targeted drug delivery, Biomaterials 30 (2009) 859–866.
[38] M.H. Hong, S.J. Zhu, Y.Y. Jiang, G.T. Tang, Y.Y. Pei, Efficient tumor targeting of hydroxycamptothecin loaded PEGylated ninosomes modified with transferrin, J. Control. Release 133 (2009) 96–102.
[39] H. Yuan, J. Miao, Y.Z. Du, J. You, F.Q. Hu, S. Zeng, Cellular uptake of solid lipid nanoparticles and cytotoxicity of encapsulated paclitaxel in A549 cancer cells, Int. J. Pharm. 348 (2008) 137–145.
[40] A.S. Ham, M.R. Cost, A.B. Sassi, C.S. Dezzutti, L.C. Rohan, Targeted delivery of PSC-RANTES for HIV-1 prevention using biodegradable nanoparticles, Pharm. Res. 26 (2009) 502–511.
[41] E.V. Batarkova, S. Li, S.V. Vinogradov, V.Y. Alakhov, D.W. Miller, A.V. Kabanov, Mechanism of Pluronic effect on P-glycoprotein efflux system in blood–brain barrier: contributions of energy depletion and membrane fluidization, J. Pharmacol Exp. Ther. 299 (2001) 483–493.
[42] J.A. Zastre, J.K. Jackson, W. Wong, H.M. Burt, P-glycoprotein efflux inhibition by amphiphilic diblock copolymers: relationship between copolymer concentration and substrate hydrophobicity, Mol. Pharm. 5 (2008) 643–653.
[43] E.V. Batrakova, S. Li, W.F. Elmquist, D.W. Miller, V.Y. Alakhov, Mechanism of sensitization of MDR cancer cells by Pluronic block copolymers: selective energy depletion, Br. J. Cancer 85 (2001) 1987–1997.
[44] N. Shaik, N. Giri, W.F. Elmquist, Investigation of the micellar effect of Pluronic P85 on P-glycoprotein inhibition: cell accumulation and equilibrium dialysis studies, J. Pharm. Sci. 98 (2009) 4170–4190.
[45] P.X. Petit, H. Lecoeur, E. Zorn, C. Dauguet, B. Mignotte, M.L. Gougeon, Alterations in mitochondrial structure and function are early events of dexamethasone-induced thymocyte apoptosis, J. Cell Biol. 130 (1995) 157–167.
[46] P.X. Petit, N. Zamzami, J.L. Vayssiere, B. Mignotte, G. Kroemer, M. Castedo, Implication of mitochondria in apoptosis, Mol. Cell. Biochem. 174 (1997) 185–188.
[47] D.R. Green, J.C. Reed, Mitochondria and apoptosis, Science 281 (1998) 1309–1312.
[48] R.C. Duke, D.M. Ojcius, J.D. Young, Cell suicide in health and disease, Sci. Am. 275 (1996) 80–87.
[49] H.C. Lee, Y.H. Wei, Mitochondrial role in life and death of the cell, J. Biomed. Sci. 7 (2000) 2–15.
[50] N. Rapoport, W.G. Pitt, H. Sun, J.L. Nelson, Drug delivery in polymeric micelles: from in vitro to in vivo, J. Control. Release 91 (2003) 85–95.
[51] N.S. Melik-Nubarov, O.O. Pomaz, T.Y. Dorodnych, G.A. Badum, A.L. Ksenofontov, O.B. Schemchukova, S.A. Arzhakov, Interaction of tumor and normal blood cells with ethylene oxide and propylene oxide block copolymers, FEBS Lett. 446 (1999) 194–198.
[52] J. Liebmann, J.A. Cook, J.B. Mitchell, Cremophor EL solvent for paclitaxel and toxicity, Lancet. 342 (1993) 1428.
[53] J. Liebmann, J.A. Cook, C. Lipschultz, D. Teague, J. Fisher, J.B. Mitchell, The influence of Cremophor EL on the cell cycle effects of paclitaxel (Taxol) in human tumor cell lines, Cancer Chemother. Pharmacol. 33 (1994) 331–339.
[54] M.A. Jordan, R.J. Toso, D. Thrower, L. Wilson, Mechanism of mitotic block and inhibition of cell proliferation by Taxol at low concentrations, Proc. Natl. Acad. Sci. USA 90 (1993) 9552–9556.
[55] E.V. Batrakova, S. Li, V.Y. Alakhov, D.W. Miller, A.V. Kabanov, Optimal structure requirements for pluronic block copolymers in modifying P-glycoprotein drug efflux transporter activity in bovine brain microvessel endothelial cells, J. Pharmacol. Exp. Ther. 304 (2003) 845–854.
[56] T. Minko, E.V. Batrakova, S. Li, Y.L. Li, R.I. Pakunlu, V.Y. Alakhov, A.V. Kabanov, Pluronic block copolymers alter apoptotic signal transduction of doxorubicin in drug-resistant cancer cells, J. Control. Release 105 (2005) 269–278.
[57] K. Sharma, L. Zhang, S. Li, D.L. Kelly, V.Y. Alakhov, E.V. Batrakova, A.V. Kabanov, Prevention of MDR development in leukemia cells by micelle-forming polymeric surfactant, J. Control. Release 131 (2008) 220–227.
[58] D.D. Guo, H.S. Moon, R. Arote, J.H. Seo, J.S. Quan, Y.J. Choi, C.S. Cho, Enhanced anticancer effect of conjugated linoleic acid by conjugation with Pluronic F127 on MCF-7 breast cancer cells, Cancer Lett. 254 (2007) 244–254.
[59] D.D. Guo, C.X. Xu, J.S. Quan, C.K. Song, H. Jin, D.D. Kim, Y.J. Choi, M.H. Cho, C.S. Cho, Synergistic anti-tumor activity of paclitaxel-incorporated conjugated linoleic acid-coupled poloxamer thermosensitive hydrogel in vitro and in vivo, Biomaterials 30 (2009) 4777–4785.
[60] F. Ahmed, R.I. Pakunlu, A. Brannan, F. Bates, T. Minko, D.E. Discher, Biodegradable polymersomes loaded with both paclitaxel and doxorubicin permeate and shrink tumors by inducing apoptosis in proportion to accumulated drug, J. Control. Release 116 (2006) 150–158.
[61] S.S.W. Ng, M.S. Tsao, S. Chow, D.W. Hedley, Inhibition of phosphatidylinositide 3-kinase enhances gemcitabine-induced apoptosis in human pancreatic cancer cells, Cancer Res. 60 (2000) 5451–5455.
[62] H. Gelderblom, J. Verweij, K. Nooter, A. Sparreboom, Cremophor EL: the drawbacks and advantages of vehicle selection for drug formulation, Eur. J. Cancer 37 (2001) 1590–1598.
[63] Sparreboom, L. van Zuylen, E. Brouwer, W.J. Loos, P. de Bruijn, H. Gelderblom, M. Pillay, K. Nooter, G. Stoter, J. Verweij, Cremophor EL-meidated alteration of paclitaxel distribution in human blood: clinical pharmacokinetic implications, Cancer Res. 59 (1999) 1454–1457.
[64] L.M. Han, J. Guo, L.J. Zhang, Q.S. Wang, X.L. Fang, Pharmacokinetics and biodistribution of polymeric micelles of paclitaxel, Acta. Pharmacol. Sin. 27 (2006) 747–753.
[65] Y.Z. Wang, Y.J. Li, L.J. Zhang, X.L. Fang, Pharmacokinetics and biodistribution of paclitaxel-loaded Pluronic P105 polymeric micelles, Arch. Pharm. Res. 31 (2008) 530–538.
[66] A.V. Kabanov, E.V. Batrakova, V.Y. Alakhov, Pluronic block copolymers as novel polymer therapeutics for drug and gene delivery, J. Control. Release 82 (2002) 189–212.
[67] K. Ueda, Y. Kawaguchi, S. Iwakawa, Effect of oxyethylene numbers on the pharmacokinetics of menatetrenone incorporated in oil-in-water lipid emulsions prepared with polyoxyethylene–polyoxypropylene block copolymers and soybean oil in rats, Biol. Pharm. Bull. 31 (2008) 2283–2287.
[68] E.V. Batrakova, S. Li, Y.L. Li, V.Y. Alakhov, W.F. Elmquist, A.V. Kabanov, Distribution kinetics of a micelle-forming block copolymer Pluronic P85, J. Control. Release 100 (2004) 389–397.
[69] M. Grindel, T. Jaworski, O. Piraner, R.M. Emanuele, M. Balasubramanian, Distribution, metabolism, and excretion of a novel surface-active agent, purified poloxamer 188, in rats, dogs, and humans, J. Pharm. Sci. 91 (2002) 1936–1947.
[70] L.C. Chang, Y.Y. Chang, C.S. Gau, Interfacial properties of Pluronics and the interactions between Pluronics and cholesterol/DPPC mixed monolayers, J. Colloid Interface Sci. 322 (2008) 263–273.